CHAPTER IV

VERTICAL TWO-PHASE FLOW REGIMES AND PRESSURE GRADIENTS UNDER THE INFLUENCE OF PIPE DIAMETER SIZES

Supachai Chootongchai[a], Anuvat Sirivat[a,*],

James O. Wilkes[b]

[a]*The Petroleum and Petrochemical College, Chulalongkorn University, Bangkok*

10330, THAILAND

[b]*Department of Chemical Engineering, The University of Michigan, Ann Arbor,*

MI 48109-2136, U.S.A

4.1 Abstract

The effect of pipe diameter size on the two-phase gas/liquid flows regimes, pressure gradients, bubble sizes and velocities was investigated. Experiment was carried out in three vertical transparent tubes with inner diameters of 10.75, 19, and 53.15 mm and the length of 3 m. Water was used as the working fluids. The boundaries of the flow regimes for a given Re_{water} increase nonlinearly with increasing tube diameter. The friction factors or the dimensionless pressure gradients are different depending on diameter. The differences may be traced back to the differences in the bubble/slug sizes and of the Eotvos number, Eo. The normalized bubble or slug dimension for pipe diameter of 10.75 mm is always greater than those of the pipe diameter of 19 mm and 53.15 mm at any Re_{air} and Re_{water}. The normalized bubble and slug velocities of pipe diameter 10.75 are always greater than those of pipe diameter of 19 mm and 53.15 mm.

Key-words: Vertical two-phase flow, three columns, pressure gradients, bubble/slug sizes, bubble/slug velocity, flow regimes

*Corresponding author: email anuvat.s@chula.ac.th, Ph: 662 218 4131, Fax: 662 611 7221

4.2 Introduction

Two-phase gas-liquid flow in a vertical tube has been well studied because of its importance in the designs of the wellhead pressure and the tube sizing, as proposed by Hewitt (2005). There are four mainly flow regimes as dictated by variation in the gas and liquid flow rates: the bubble, the slug, the annular, and the mist regimes. Characteristics of the flow regimes depend on several factors: the individual magnitudes of the liquid and gas flow rates and the pipe diameter; the physical properties of liquid and gas, such as temperature, pressure, density, viscosity, and surface tension. Each flow regime may influence at different degrees the heat transfer rate, the momentum transfer, the energy loss and the energy exchange rate, and the pressure gradient.

The behavior of a single gas bubble released in a column of liquid within in a vertical tube depends on the size of the bubble. When the bubble is quite small, it remains spherical and rises along a vertical rectilinear path. Larger bubbles become ellipsoidal or irregularly shaped and tend to rise along helical or zigzag paths. With increasing gas flow rate, large cap-shaped bubbles are formed by collisions. When the diameter of the bubbles is nearly the same as the tube diameter, it is the initiation of the slug flow. The churn flow, a transition between the slug and annular regimes, is highly disturbed and has large waves flowing up the channel, interspersed with regions of falling liquid films. In the annular flow, part of it is the liquid film and the rest is dispersed in the gas core in the form of fine droplets. With increasing gas flow rate, the liquid film will be thinner while the number of droplets increases. The mist flow starts when the liquid film is removed from the wall. Detailed characteristics and measuring methodology of various flow regimes of the two-phase liquid and gas flow can be found from the previous works of Lockhart and Martinelli (1949), Davies and Taylor (1950), Nicklin (1962), Wallis (1969), Sylvester (1987) and Wilkes (1999).

Fukano and Kariyasaki (1993) investigated the characteristics of the air-water isothermal two-phase flow in capillary tubes with the inner diameters of 1 mm, 2.4 mm, 4.9 mm, and 9 mm. The directions of flow were vertical upward, horizontal and vertical downward. Capillary force was important in the case the tube inner diameter was less than 5 mm - 9 mm. Flow patterns remained the same regardless of the flow direction.

Colin and Fabre (1995) studied the influence of tube diameter in microgravitational two-phase flows. The experiments were carried out in 6, 10 and 19 mm inner diameter tubes and a comparison was made with the previous results obtained from a 40 mm inner diameter tube. In the 40 mm tube, a strong tendency to coalescence led to a rapid transition to slug flow, whereas coalescence was much weaker in the smaller tubes. The bubbly flow was found at void fractions up to 0.45. Pressure drop and the wall friction factor were also strongly affected by tube diameter.

Xin et al. (1996) investigated the pressure drop in an air-water two-phase flow in vertical helicoidal pipes. The coil diameter and pipe diameter had no apparent effect on the void fraction, but they had some effect on the frictional pressure drop.

Cheng et al. (1998) studied of the bubble up to the slug transition regime in a vertical gas-liquid flow with tube diameter ranging 28.9 mm-150 mm. The data indicate that the traditional slug flow did not exist in the 150 mm diameter tube. Instead, there was a very gradual transition to the churn flow as the gas rate was increased.

Coleman and Garimella (1999) studied the effect of tube diameter and shape on the flow regime transitions for a two-phase flow in tubes with small hydraulic diameters ranging from 5.5 to 1.3 mm. Gas and liquid superficial velocities were varied from 0.1 to 100 ms^{-1}, respectively. As the tube diameter decreased, transitions between flow regimes occurred at different combinations of superficial gas and liquid velocities. Decreasing the tube diameter shifted the transition of the dispersed flow regime towards a higher superficial liquid velocity value due to the combined effects of surface tension and tube diameter.

Hajiloo *et al.* (2001) studied the effect of tube diameter (inner diameter ranging from 1.56 - 4.12 cm) on the downward co-current annular two-phase flow with the water and air Reynolds numbers in the ranges of 5100-27200 and 3400-21600, respectively. At a fixed gas Reynolds number, a large increase in friction was accompanied by a decrease in tube diameter.

In our work, we are interested in investigating the effect of pipe diameter on the flow regimes, the corresponding pressure gradients, the bubble/slug size, and the bubble/slug velocity of a vertical two-phase flow.

4.3 Experimental Apparatus

The experimental setup is shown schematically in Figure 1. Air and water were used as the working fluids. The main components of the system consist of the vertical test section, an air supply, water supply and instrumentation. Three pipes with three different inside diameters (10.75, 19, 53.15 mm) each having a length of 3 m were used. The pipes were made from transparent acrylic glass to permit visual observation of the flow patterns. At the bottom of the test columns, there was an inlet for the compressed air from a compressor (Taiwan, Fu Sheng HTA-100H) and flow rates were measured by calibrated air-rotameters ((1) Cole-Parmer, A-32466-66, U.S.A., (2) Cole-Parmer, A-32466-68, U.S.A., (3) Cole-Parmer, A-32466-70, U.S.A.). Water was pumped from the storage tank through a rotameter and mixed with air at the bottom of the test column. The flow rate of the liquid was measured by a calibrated liquid-rotameter (Cole-Parmer, U.S.A, A-32461-42). Liquid flowed upward through the main column with air and then flowed back to the storage tank. Two static pressure tabs in each column were installed at two axial locations with spacing of 0.4 m and were connected to a manometer which was used to measure the pressure drops along the test section. The physical properties of the water used in the experiment are listed in Table 1.

Experiments were conducted by varying the air and liquid flow rates. The air flow rate was increased by small increments as the water flow rate was kept constant. The experimental conditions were as follows: air Reynolds number Re_{air}: 3.14-71,275, water Reynolds number Re_{water}: 0-2,740. Definitions of Re_{air} and Re_{water}

are defined in Table 1. Air and water temperatures were between ~31-32°C. The system was allowed to approach the steady condition before data were taken. The pressure drops across the test section were measured at different flow rates of air and liquid; average values were computed and reported from at least 5 readings. The flow regimes were observed and identified by visual observation: a video camera (Panasonic, NV-M3000) and a software program (Snagit 8.0). Bubble size, slug size, and void fraction of the Taylor bubble were identified and measured by a software program (Scion Image). Bubble velocity was measured by timing bubbles traveling past known distances. Bubble and Taylor sizes and velocity were measured from 3-5 samples, and average values were computed and reported.

4.4 Results and Discussion

<u>Visual Observations of the Flow Regimes by Photographs</u>

The air flow rate was increased while the liquid flow rate was kept fixed. Boundaries of the flow regimes were identified to be the transitions towards the bubble-slug, the slug, the slug-churn, the churn, the annular, and the mist regimes, respectively. Each flow regime boundary was identified by visual observations through the video camera. The critical Reynolds numbers of air $(Re_{air})_{critical}$ for each flow regime of the three tubes were identified. For $Re_{water} = 0$, $Re_{air,critical}$ for the bubble-slug and the slug flow regimes are; 5.6 and 14.35 for the pipe diameter of 10.75 mm, 10.59 and 22.95 for the pipe diameter of 19 mm, and 132 and 289 for the pipe diameter of 53.15 mm. $Re_{air,critical}$ for the bubble-slug and slug flow regimes appear increase nonlinearly with tube diameter. Similar nonlinear increases in $Re_{air,critical}$ for other regimes and at other Re_{water} values of ~1,000 and ~2,700 also occur; values are tabulated in Table 2

Effect of Tube Sizes on the Pressure Gradients

Figures 2(a) to 2(c) show the dynamic pressure gradients, $(-dp/dz)_d$, vs. air Reynolds number, Re_{air}, for the three tubes at $Re_{water} = 0$, $\sim 1,000$ and $\sim 2,700$. The dynamic pressure gradients are defined by the following relation:

$$(-\frac{dp}{dz})_d = (\frac{\Delta P}{L})_d = (\frac{\Delta P}{L})_m + \rho_w g, \tag{1}$$

where $(\frac{\Delta P}{L})_m$ is the measured pressure gradient along a distance L between the pressure taps, ρ_w is the water density, and g is the gravity. $(\frac{\Delta P}{L})_m$ is the dynamic pressure gradient. Figure 2(a) shows that at $Re_{water} = 0$ the dynamic pressure gradient for the pipe with diameter of 10.75 mm is higher than those of the pipes with diameters of 19 mm and 53.15 mm. The pressure gradients for the three diameters increase steadily with increasing Re_{air}.

In Figures 2(b) and 2(c) at $Re_{water} = 1,000$ and 2,700, the dynamic pressure gradients of the three diameters increase monotonically from the bubble flow regime to the slug flow regime. In the churn flow regime, the dynamic pressure gradients appear to remain constant. On the other hand, in the annular flow and the mist flow regimes, the dynamic pressure gradients decrease with increasing Re_{air}. For the pipes of diameters of 10.75 mm and 19 mm in the bubble and the slug flow regimes, the dynamic pressure gradients are comparable in magnitude. In the annular and the mist flow regimes, the dynamic pressure gradient for the pipe diameter of 19 mm is evidently much higher than that of the pipe with diameter of 10.75 mm.

Finally, we may note from Figures 2(a)-2(b) that for the pipe with diameter of 53.15 mm, the pressure gradient of the air-liquid two phase flows are constant and independent of Re_{air} provided it is less than 10, when $Re_{liquid} \sim 0$ and 1,000.

Figures 3(a) to 3(b) show the dimensionless pressure gradient, $2d(-dp/dz)_d/\rho_w u_l^2$, vs. air Reynolds number, Re_{air}, at fixed $Re_{water} = \sim 1,000$ and $\sim 2,700$. We define the dynamic wall shear stress ($\tau_{w,d}$):

$$\frac{d}{4}(\frac{\Delta P}{L})_d = \tau_{w,d}, \tag{2}$$

where $(\frac{\Delta P}{L})_d$ is the dynamic pressure gradient along a distance L between the pressure taps. From the definition of the Darcy friction factor (f_F) (Wilkes (1999)):

$$f_F = \frac{8\tau_{w,d}}{\rho_w \overline{u}_{liq}^2}, \tag{3}$$

where $\overline{u}_{liq}$ is mean liquid velocity defined as

$$\overline{u}_{liq} = \frac{4Q_L}{\pi d^2}. \tag{4}$$

The friction factor for a two phase flow can be written in terms of the dimensionless pressure gradient the friction factor as:

$$f_F = \frac{2d(-\frac{dp}{dz})_d}{\rho_w \overline{u}_{liq}^2}. \tag{5}$$

Figures 3(a)-3(b) shows the dimensionless pressure gradients vs. Re_{air} at Re_{water} ~1,000 and 2,700. Typically, the friction factor as defined in Eqs (4)-(5) increases monotonically with Re_{air} for the bubble to the churn flow regimes; the slight decreases appear for the annular and the mist flow regimes because the decreases in the liquid contact with the wall. The important fact to be noted from Figures 3(a)-3(b) is that the friction factors or the dimensionless pressure gradients are different amongst the three diameters. The differences may be traced back to the differences in the bubble/slug sizes and the Eo number. Eo is defined as the ratio between the gravity force over the surface tension, $Eo = \rho g d^2 / \gamma$. In our work, the Eo numbers are 15.83, 49.44, 387 corresponding the pipe diameters of 10.75, 19, and 53.15, respectively.

Effect of Tube Sizes on the Bubble and Slug Sizes

Figures 4(a) to 4(c) show photographs of the bubbles in water at $Re_{water} = 0$ and at nearly the same $Re_{air} \sim 3$. In Figure 4(a): $Re_{air} = 3.41$, pipe diameter is 10.75 mm, and Eo = 15.83. In Figure 4(b): $Re_{air} = 3.17$, pipe diameter is 19 mm, and Eo = 49.44. Lastly in Figure 4(c): $Re_{air} = 2.9$, pipe diameter is 53.15 mm, and Eo = 387. The shape of the bubbles appear as a spherical cap with a cylinder, a spherical cap, and a blunt nose bubble, corresponding to Eo = 15.8, 49.4, and 387, respectively.

Figures 5(a) to 5(c) show the normalized bubble widths, w_b/d, vs. air Reynolds number, Re_{air}, at $Re_{water} = 0$, ~1,000 and ~2,700, respectively. It can be seen that the normalized bubble width, w_b/d, for the pipe diameter of 10.75 mm is greater than those of the pipe diameters of 19 mm and 53.15 mm at any Re_{air} or Re_{water}. This finding suggests that for the same air volume flow rate or Re_{air}, a relative more space filling bubble in a smaller pipe diameter can be expected.

Figures 6(a) to 6(c) show the normalized bubble heights, R_h/d, vs. air Reynolds number, Re_{air}, at fixed Re_{water} equal to 0, ~1,000 and ~2,700. The normalized bubble height increases monotonically with increasing Re_{air}, as to be expected with increasing air flow rate. From these figures, it can be seen that the normalized bubble height for pipe diameter of 10.75 mm is higher than those of pipe diameters of 19 mm and 53.15 mm at any Re_{air} and Re_{water}.

Figures 7(a) to 7(c) show the normalized slug heights, L_{TB}/d, vs. air Reynolds number, $Re_{air.}$, at $Re_{water} = 0$, ~1,000 and ~2,700, respectively. The normalized slug height increases monotonically with increasing Re_{air}. The normalized slug height of pipe diameter of 10.75 is always greater than those of pipe diameters of 19 mm and 53.15 mm. at any Re_{air} and $Re_{water.}$

In summary, we have shown that the normalized bubble widths, and heights, and the normalized slug length vary with the pipe diameter or Eo number, implying the effect of gravity and the conservation of air mass.

Effect of Tube Size on the Bubble and Slug Velocities

In our work, the bubble and slug velocities are normalized as $\dfrac{u}{\sqrt{gd}}$.

Figures 8(a) to 8(c) show the normalized bubble and slug velocities, $\dfrac{u}{\sqrt{gd}}$,
vs. air Reynolds number, Re_{air}, at $Re_{water}= 0, \sim1000, \sim2700$. In these figures, it can
be seen that the normalized bubble and slug velocities increase monotonically with
Re_{air}, satisfying the conservation of air mass. In Figure 8(a), at $Re_{water} \sim 0$, the
normalized bubble and slug velocities vs. Re_{air} of pipe diameter 19 mm are nearly the
same as 53.15 mm. The normalize bubble velocity of pipe diameter 10.75 mm is
lower than those of pipe diameters 19 mm and 53.15 mm. On the other hand, the
normalized slug velocity of pipe diameter 10.75 mm is greater than those of pipe
diameters 19 mm and 53.15 mm. In Figures 8(b) and 8(c), at $Re_{water} \sim1,000$ and
$\sim2,700$, the bubble and slug velocities of pipe diameter 10.75 mm are greater than
those of pipe diameters 19 mm and 53.15 mm, again reflecting the conservation of
air mass.

4.5 Conclusions

The experiments were carried out in the two-phase upward flows in three
pipes with three different inside diameters (10.75, 19, 53.15 mm) each having a
length of 3 m. Air-water were used as the working fluid. The influences of pipe
diameter on the flow regimes, the pressure gradients, the bubble/slug size, the
bubble/slug velocity are investigated.

The boundaries of the flow regimes for the same Re_{water} increase nonlinearly
with increasing tube diameters.

The dynamic pressure gradients for the pipes diameter of 10.75 mm and 19
mm are comparable in magnitude for the bubble and the slug flow regimes. In the
churn flow regime, the dynamic pressure gradients for the pipes diameter of 10.75
mm and 19 mm appear to remain constant. For the annular and the mist flow

regimes, the dynamic pressure gradient for **pipe** diameter of 19 mm is higher than pipe diameter of 10.75 mm. For the pipe with diameter of 53.15 mm, the pressure gradients are independent of Re_{air} provided it is less than 10. The friction factors or the dimensionless pressure gradients are different amongst the three diameters. The differences may due to the differences in the bubble/slug sizes and the Eo.

The normalized bubble and slug dimension for each pipe diameter increase monotonically with increasing Re_{air} implying effect from the air flow rate. For the pipe diameter of 10.75 mm is always greater than those of the pipe diameters of 19 mm and 53.15 mm at any Re_{air} and Re_{water}.

The normalized bubble and slug velocities increase monotonically with Re_{air}, implying the conservation of air mass. At high Re_{water} the bubble and slug velocities of pipe diameter 10.75 mm are always greater than those of pipe diameter of 19 mm and 53.15 mm, again reflecting the conservation of air mass.

4.6 Acknowledgements

4.7 References

Barbosa, J.R., Govan, A.H., Hewitt, G.F., 2001. Visualisation and modelling studies of churn flow in a vertical pipe. International Journal of Multiphase Flow 27, 2105-2127.

Cachard, F., Delhaye, J.M., 1996. A slug-churn flow model for small-diameter airlift pumps. International Journal of Multiphase Flow 22(4), 627-649.

Cheng, H., Hills, J.H., Azzorpardi, B.J., 1998. A study of the bubble-to-slug transition in vertical gas–liquid flow in columns of different diameter. International Journal of Multiphase flow 24(3), 431-452.

Coleman, J.W., Garimella, S., 1999. Characterization of two-phase flow patterns in small diameter round and rectangular tubes. International Journal of Heat and Mass Transfer 42, 2869-2881.

Colin, C., Fabre, J., 1995. Gas-liquid pipe flow under microgravity conditions: Influence of tube diameter on flow patterns and pressure drops. Adv. Space Res. 16(7), 137-142.

Davies, R.M., Taylor, G.I., 1950. The mechanics of large bubbles rising through extended liquids and through liquids in tubes. Proceedings of Royal. Society 200A,

375-390.

Delfos, R., Wisse, C.J., Oliemans, R.V.A., 2001. Measurement of air-entrainment from a stationary Taylor bubble in a vertical tube. International Journal of Multiphase Flow 27, 1769-1787.

Duangprasert, T., 2006. Vertical two-phase flow regime and pressure gradient under the influence of SDS surfactant. MS thesis, Petroleum and petrochemical college, Chulalongkorn university, Bangkok.

Fukano, T., Kariyasaki, A., 1993. Characteristics of gas-liquid two-phase flow in a capillary tube. Nuclear Engineering and Design 141, 59-68.

Hajiloo, M., Chang, B.H., Mills, A.F., 2001. Interfacial shear in downward two-phase annular co-current flow. International Journal of Multiphase Flow 27, 1095-1108.

Hawkes, N.J., Lawrence, C.J., Hewitt, G.F., 2000. Studies of wispy-annular flow using transient pressure gradient and optical measurements. International Journal of Multiphase Flow 26, 1565-1582.

Hewitt, G.F., 2005. Three-phase gas-liquid-liquid flows in the steady and transient states. Nuclear Engineering and Design 235, 1303-1316.

Hlaing, N.D., Sirivat, A., Siemanond, K., Wilkes, J.O., 2007. Vertical two-phase flow regimes and pressure gradients: Effect of viscosity. Experimental Thermal and Fluid Science 31, 567-577.

Lockhart, R.W., Martinelli, R.C., 1949. Proposed correlation of data for isothermal two-phase, two-component flow in Pipes. Chemical Engineering Progress 45(1), 39-48.

Nicklin, D.J., 1962. Two-phase bubble flow. Chemical Engineering Science 17, 693- 702.

Sylvester, N.D., 1987. A mechanistic model for two-phase vertical slug flow in pipes. Journal of Energy Resources Technology, Transactions of the ASME 109, 206-213.

Viana, F., Pardo, R., Yanez, R., Trallero, J.L., Joseph, D.D., 2003. Universal correlation for the rise velocity of long gas bubbles in round pipes. J. Fluid Mech. 494, 379-398.

Walllis, G.B., 1969. One-dimensional Two-Phase Flow, McGraw Hill, New York.

Watson, M.J., Hewitt, G.F., 1999. Pressure effects on the slug to churn transition. International Journal of Multiphase Flow 25, 1225-1241.

Wilkes, J.O., 1999. Fluid Mechanics for Chemical Engineers, Prentice-Hall PTR, New Jersey.

White, E.T., Beardmore, R.H., 1962. The velocity of rise of single cylindrical air bubbles through liquids contained in vertical tubes. Chemical Engineering Science 17, 351-361.

Wolk, G., Dreyer, M., Rath, H.J., 2000. Flow patterns in small diameter vertical non-circular channels. International Journal of Multiphase Flow 26, 1037-1061.

Xin, R.C., Awwad, A., Dong, Z.F., Ebadian, M.A., Soliman, H.M., 1996. An investigation and comparative study of the pressure drop in air-water two-phase flow in vertical helicoidal pipes. International Journal of Heat and Mass Transfer 39(4), 735-743.

Table 1 Physical properties of the gas and the liquid used in the experiment

Gas / Liquid	v (m²/s)	μ (Pa.s)	ρ (kg/m³)	σ (μS/cm)	γ (mN/m)
Air	1.57×10^{-5}	1.85×10^{-5}	1.18	-	-
Water	8.52×10^{-7}	8.48×10^{-4}	995	1.3	71.27

v: kinematic viscosity, μ: viscosity , ρ: density, σ: electrical conductivity,

γ: surface tension, d : pipe diameter, and v : velocity

System temperature, $T = 31^{\circ}C$ ($\pm 1^{\circ}C$)

Re_{air}: air Reynolds number ($\dfrac{\rho_{air} d v_{air}}{\mu_{air}}$)

Re_{water}: water Reynolds number ($\dfrac{\rho_{water} d v_{water}}{\mu_{water}}$)

Eo : Eotvos number ($\dfrac{\rho g d^2}{\gamma}$)

Y : property parameter ($\dfrac{g \mu^4}{\rho \gamma^3}$) $= 1.41 \times 10^{-11}$

Table 2 The critical Reynolds numbers $(Re_{air})_{critical}$ of various regimes of 3 pipe diameters: 10.75, 19, and 53.15 mm

Pipe diameter (mm)	Eo	Re_{water}	$Re_{air, critical}$					
			Bubble-slug	Slug	Slug-churn	Churn	Annular	Mist
10.75	15.83	0	5.6	14.35	-	-	-	-
		1079	14.35	23.09	140	523	4554	25195
		2727	27.47	36.22	231	1427	12597	25195
19	49.44	0	10.59	22.95	-	-	-	-
		1010	15.54	33.21	296	1454	28510	57020
		2740	38.33	48.59	369	2474	28510	57020
53.15	387	0	132	289	-	-	-	-
		1028	184	445	2548	10192	-	-

1. Air compressor
   maximum 10 bar
2. Solution reservoir tank
3. Air rotameter
4. Liquid rotameter
5. Air injection valve
6. Acrylic tube (1.1 cm)
7. Acrylic tube (1.9 cm)
8. Acrylic tube (5.3 cm)
9. Overflow acrylic tube
   (5.4 cm)
10. Liquid pump
11. Liquid injection valve
12. Manometer
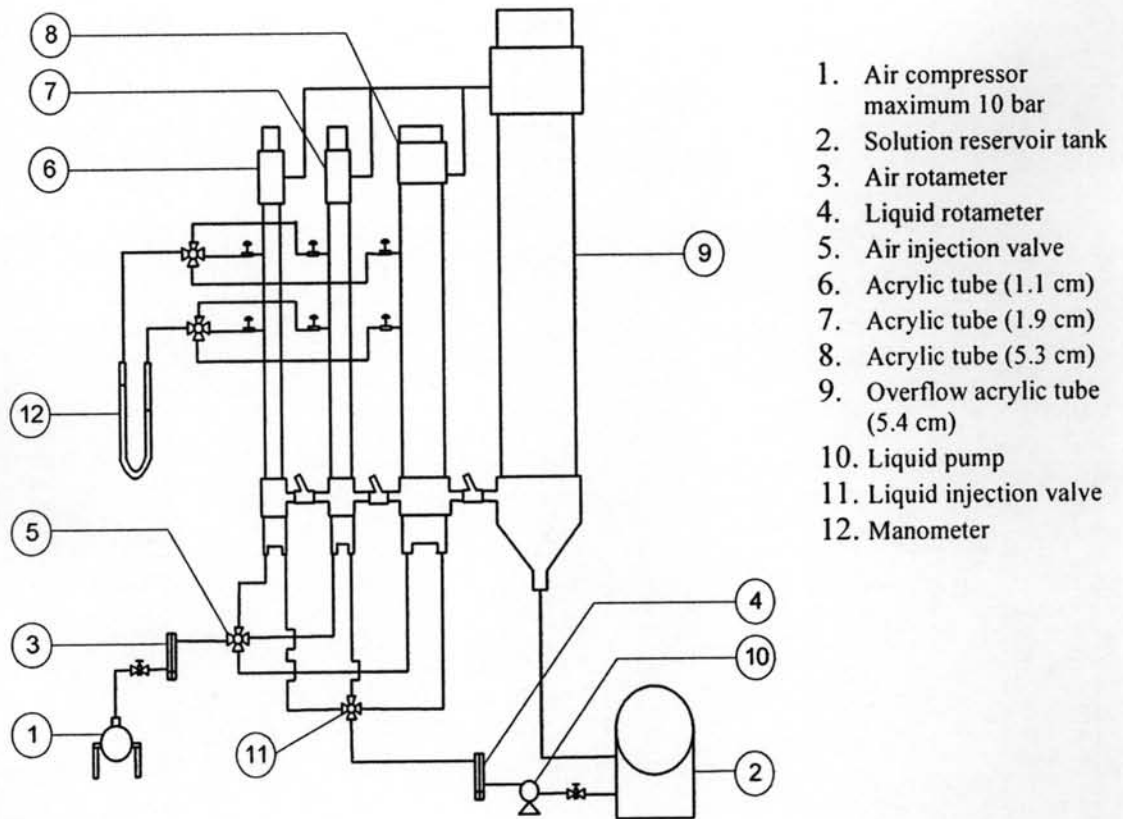
Figure 1 Schematic diagram of the experimental apparatus.

(-dp/dz)$_d$: Dynamic pressure gradient

(a)

(-dp/dz)$_d$: Dynamic pressure gradient
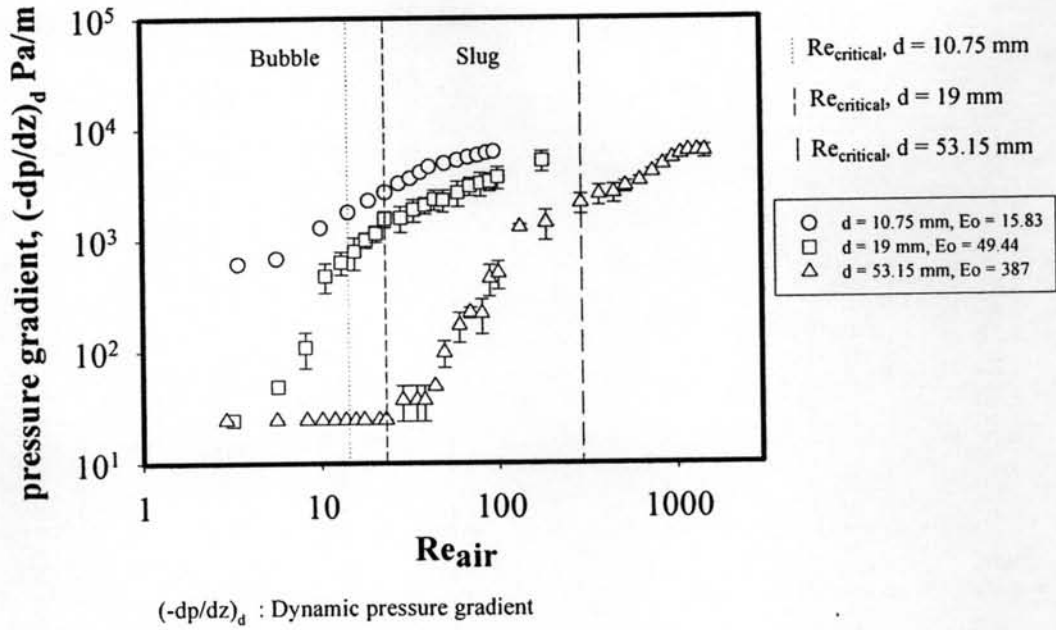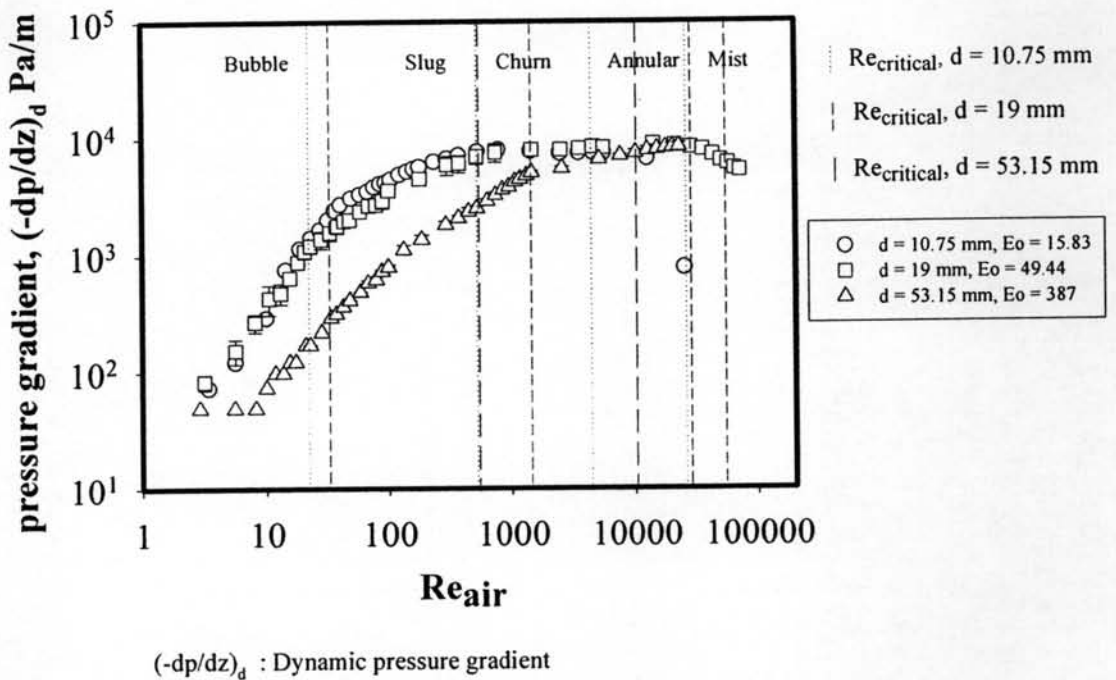
(b)
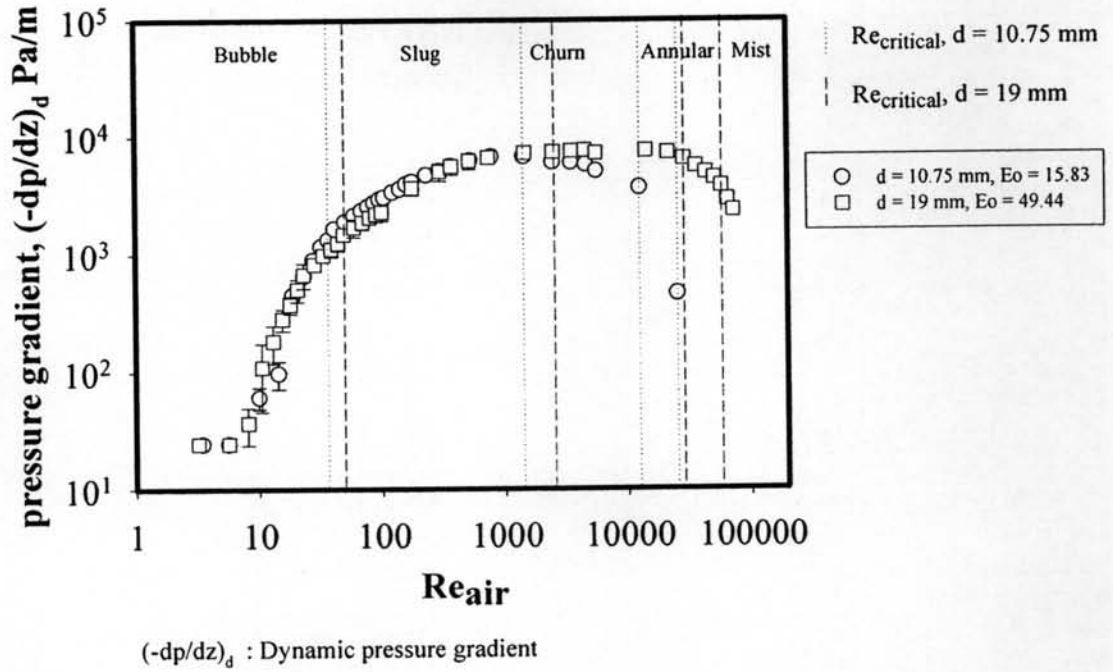
(c)

Figure 2 Effect of pipe diameter on dynamic pressure gradient: a) $Re_{water} = 0$; b) $Re_{water} = 1079$, 1010 and 1028; c) $Re_{water} = 2727$ and 2740.

pressure gradient, $2d(-dp/dz)_d/\rho_w u_l^2$ vs Re_{air}

Legend:
- $Re_{critical}$, d = 10.75 mm
- $Re_{critical}$, d = 19 mm
- $Re_{critical}$, d = 53.15 mm

- ○   d = 10.75 mm, Eo = 15.83
- □   d = 19 mm, Eo = 49.44
- △   d = 53.15 mm, Eo = 387

Flow regimes: Bubble, Slug, Churn, Annular, Mist
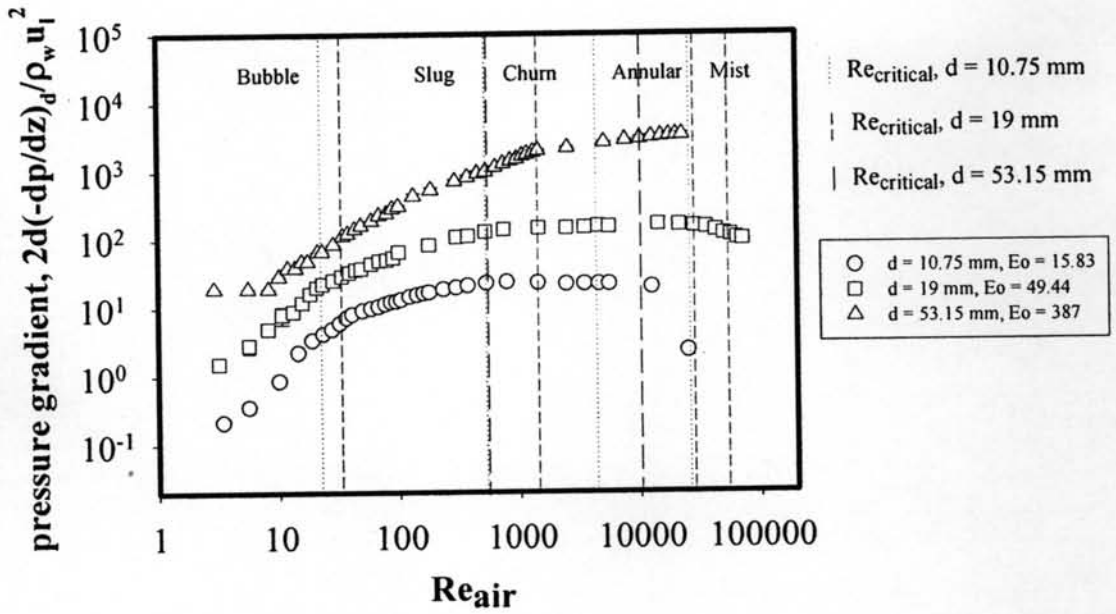
$(-dp/dz)_d$: Dynamic pressure gradient

ρ_w : Water density

u_l : liquid velocity, (Liquid flow rate / Cross section area)

(a)

(b)

Figure 3 Effect of pipe diameter on dimensionless pressure gradient: a) $Re_{water} = 1079$, 1010 and 1028; b) $Re_{water} = 2727$ and 2740.
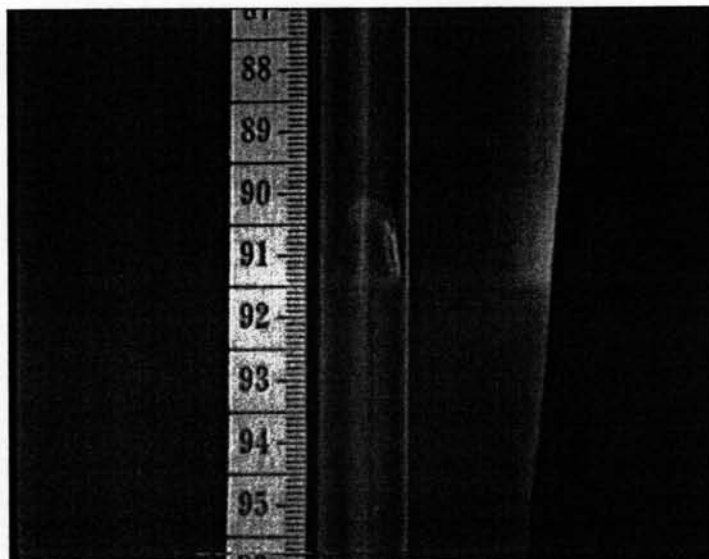
(a)
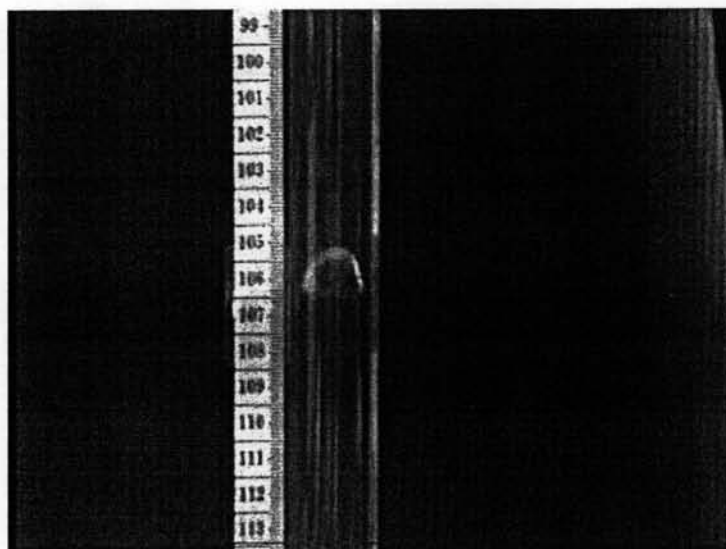
(b)
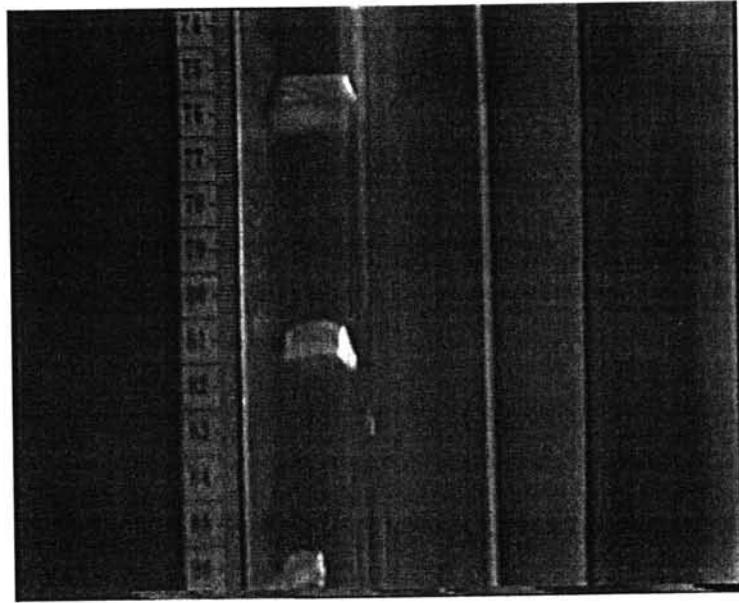
(c)

Figure 4 Photographs of bubbles in the bubble flow regime at $Re_{water} = 0$: a) $Re_{air} = 3.41$, pipe diameter of 10.75 mm, $Eo = 15.83$; b) $Re_{air} = 3.17$, pipe diameter of 19 mm, $Eo = 49.44$; c) $Re_{air} = 2.9$, pipe diameter of 53.15 mm, $Eo = 387$.

(a)

(b)
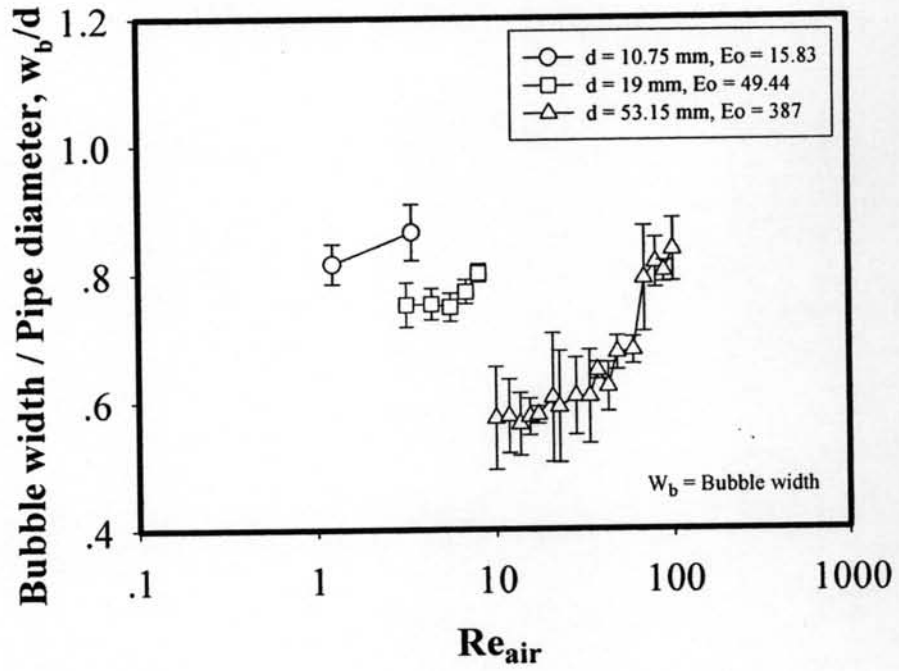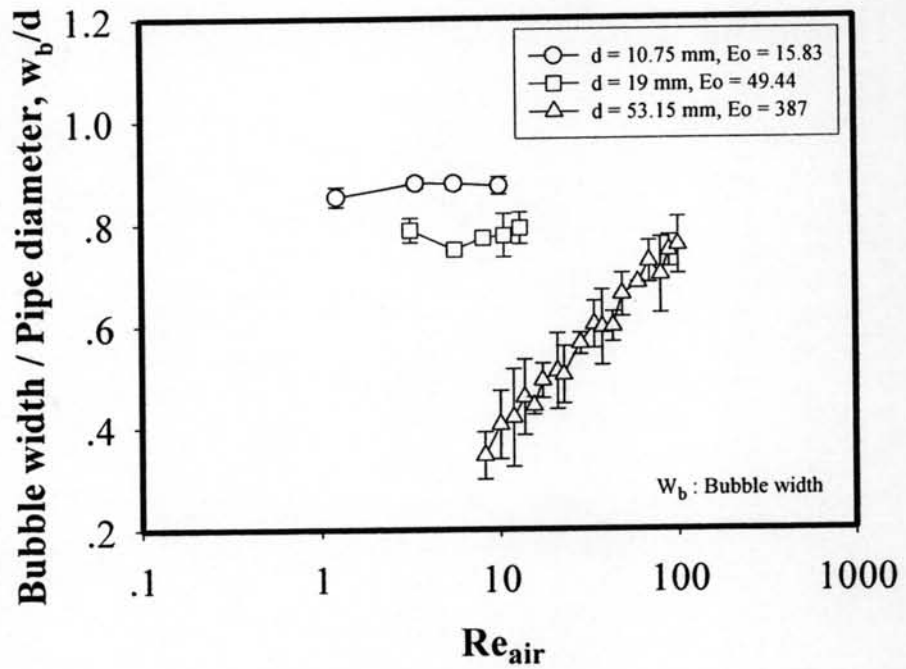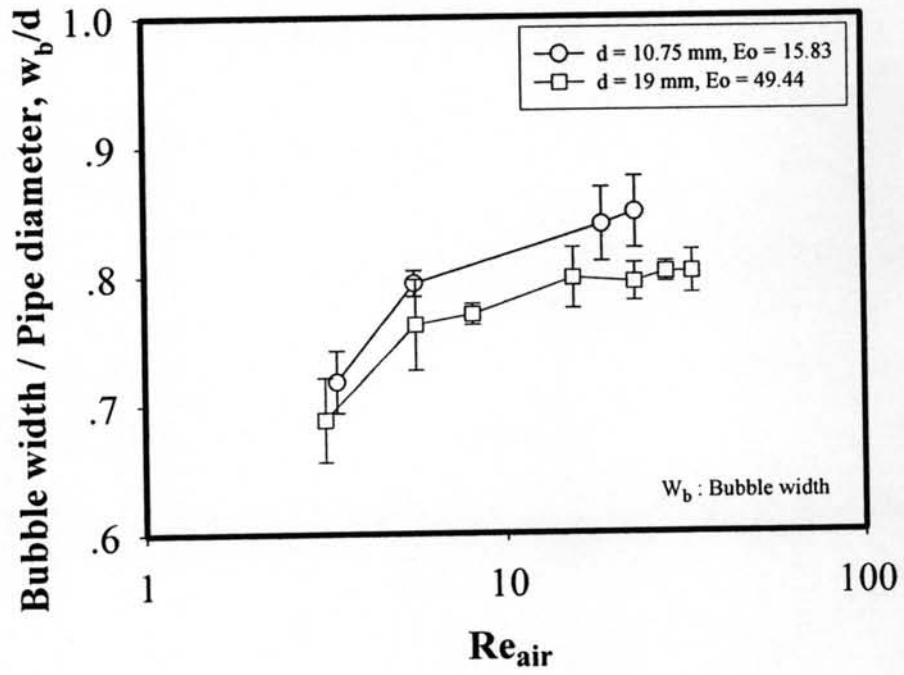
Figure 5 Effect of pipe diameter on bubble width: a) $Re_{water} = 0$; b) $Re_{water} = 1079$, 1010 and 1028; c) $Re_{water} = 2727$ and 2740.

(a)

(b)
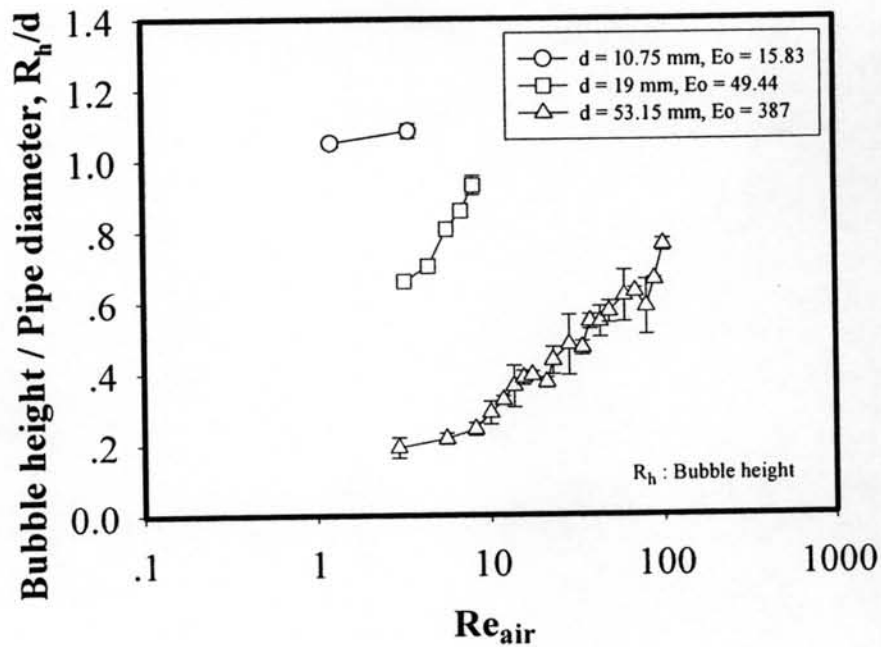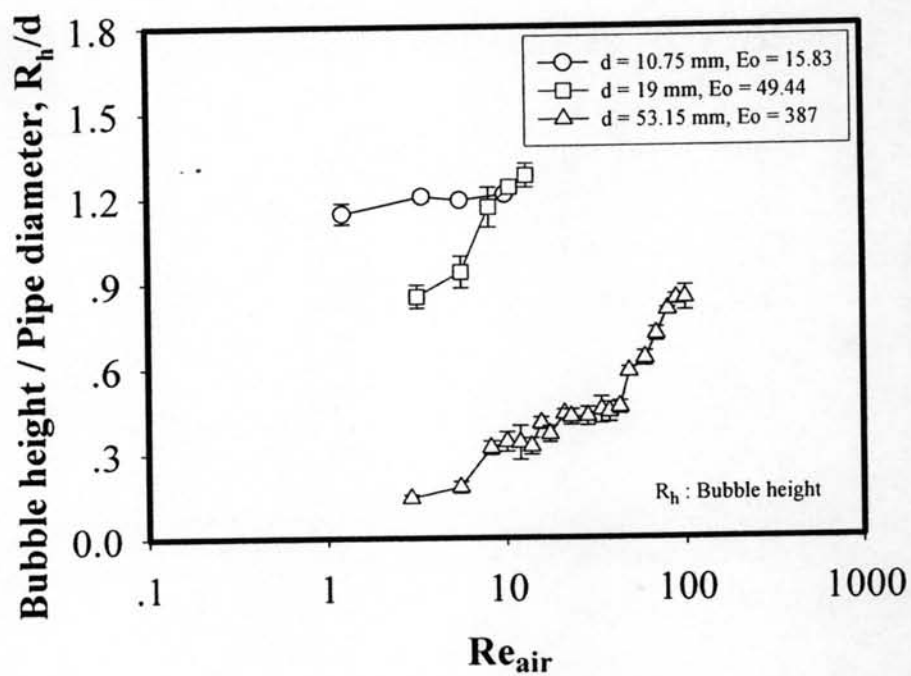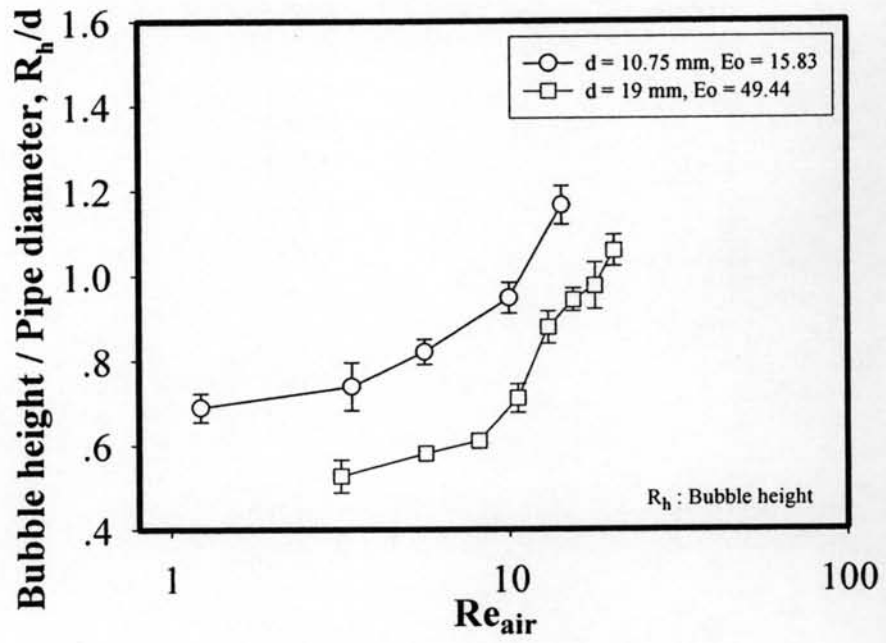
Figure 6 Effect of pipe diameter on bubble height: a) $Re_{water} = 0$; b) $Re_{water} = 1079$, 1010 and 1028; c) $Re_{water} = 2727$ and 2740.
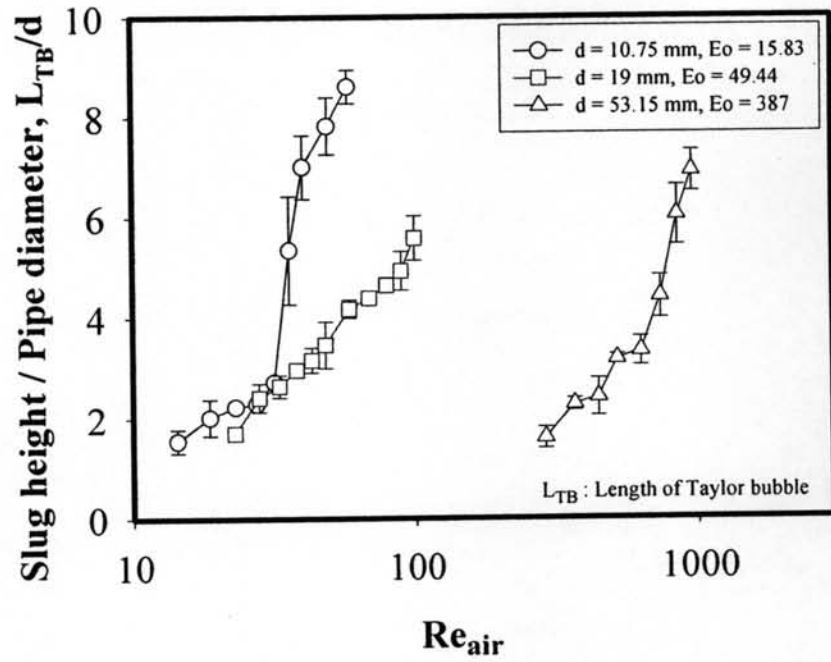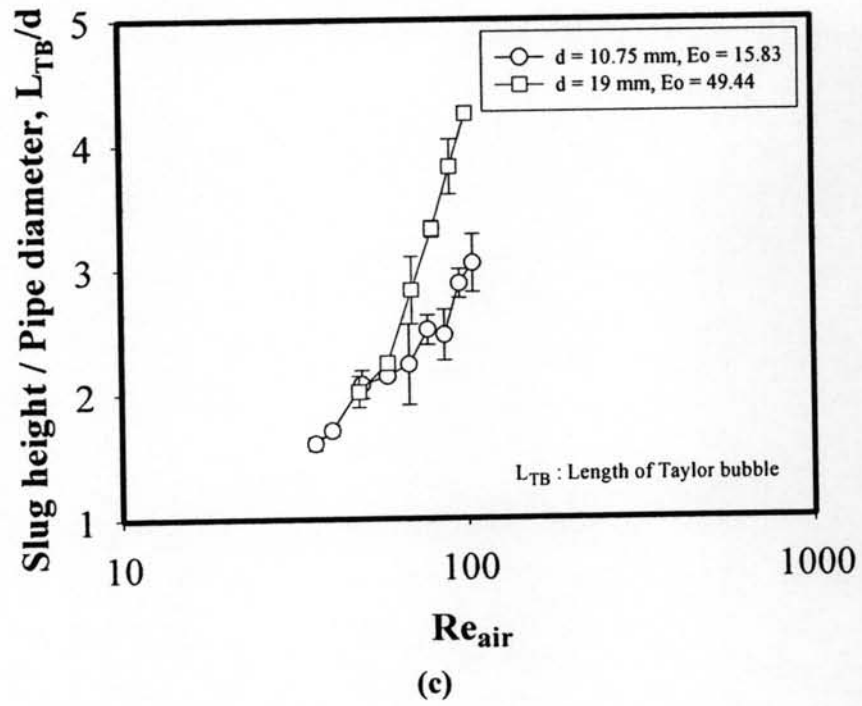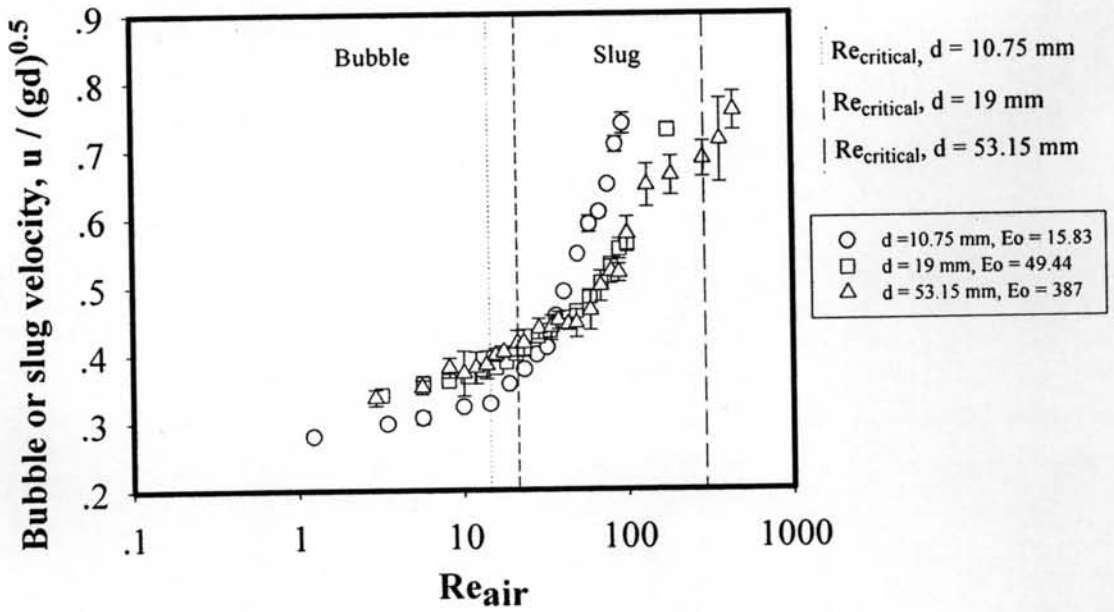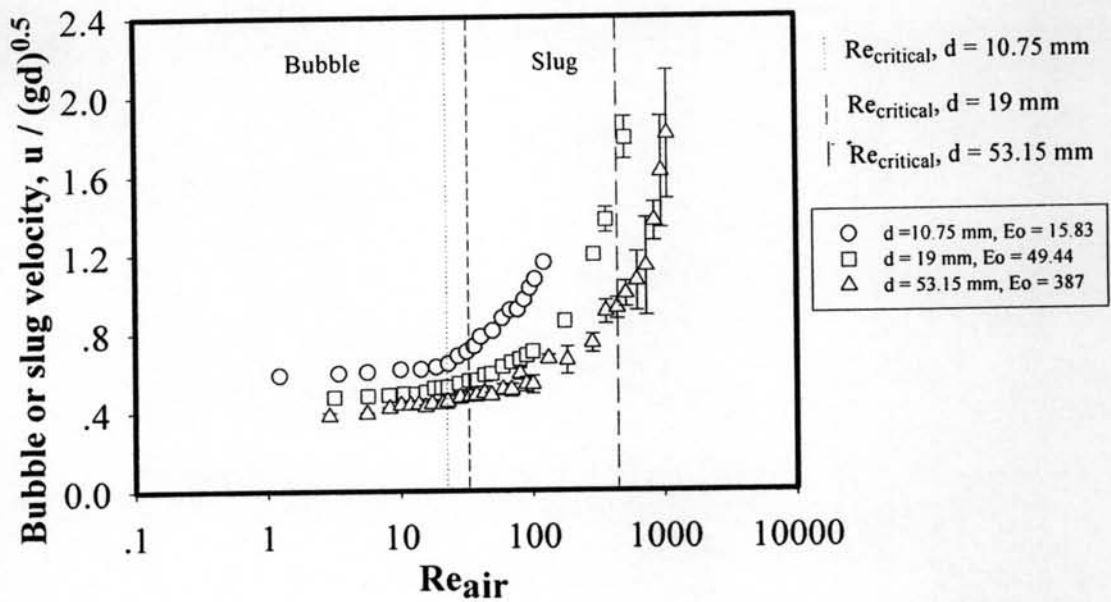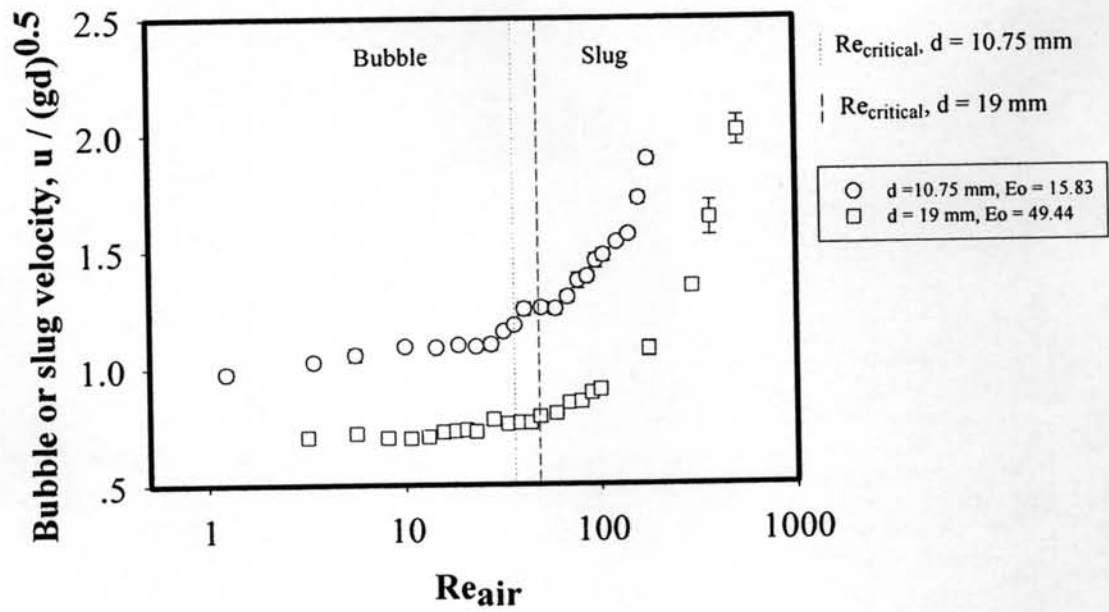
(a)
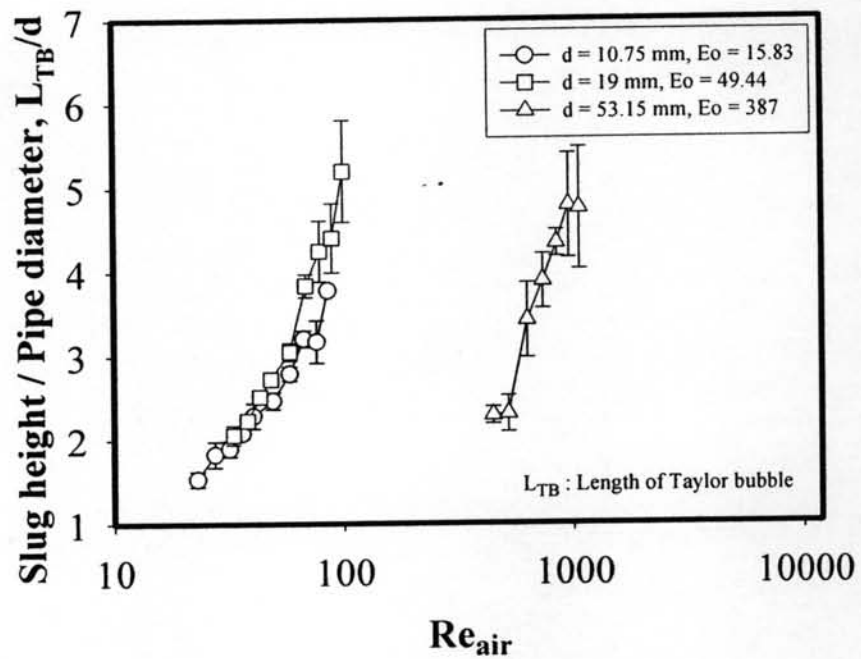
(b)

Figure 7 Effect of pipe diameter on slug height: a) $Re_{water} = 0$; b) $Re_{water} = 1079$, 1010 and 1028; c) $Re_{water} = 2727$ and 2740.

(a)

(b)

(c)

Figure 8 Effect of pipe diameter on bubble or slug velocity: a) $Re_{water} = 0$; b) $Re_{water} = 1079$, 1010 and 1028; c) $Re_{water} = 2727$ and 2740.